

# Foamability of MgAl<sub>2</sub>O<sub>4</sub> (spinel)-reinforced aluminium alloy composites

G. S. Vinod Kumar<sup>1,2\*</sup>, M. Chakraborty<sup>3</sup>, F. Garcia Moreno<sup>1,2</sup>, J. Banhart<sup>1,2</sup>

1. Technische Universität Berlin, Hardenbergstraße. 36, 10623 Berlin, Germany

2. Helmholtz-Zentrum Berlin für Materialien und Energie, Hahn Meitner Platz, 14109 Berlin,  
Germany

3. Dept. of Metallurgical and Materials Eng., Indian Institute of Technology, Kharagpur 721302, India

## Abstract

A novel foamable aluminium alloy has been developed. It contains sub- $\mu\text{m}$ -sized MgAl<sub>2</sub>O<sub>4</sub> (spinel) particles that are generated *in-situ* by a reaction of SiO<sub>2</sub> with a molten Al-Mg alloy. The study involves an optimization of parameters such as Mg concentration, SiO<sub>2</sub> particles size and reaction time and shows that a composite containing MgAl<sub>2</sub>O<sub>4</sub> particles as chief reinforcement in the matrix leads to effective foaming. Composites containing large sized transition phases and particle agglomerates in the matrix yield poor foam structure. The best foamable composite obtained contained 3.4 vol.% of ultra-fine (80 nm to 1 $\mu\text{m}$ ) MgAl<sub>2</sub>O<sub>4</sub> particles uniformly distributed in a Al-Si alloy matrix. The corresponding metal foam contained 75% porosity and exhibited a uniform distribution of cells.

Key words: aluminium foam, foam stability, MgAl<sub>2</sub>O<sub>4</sub> (spinel), metal-matrix composites

## 1. Introduction

Making closed-cell aluminium alloy foams directly from molten alloys promises to be economical as fewer processing steps are required compared to manufacturing routes based on metal powders<sup>[1]</sup>. However, ceramic or intermetallic particles are required for foam

---

\* Corresponding author's email ID: [vinodnarasimha@gmail.com](mailto:vinodnarasimha@gmail.com)

stabilisation<sup>[2-5]</sup>, which can be a disadvantage especially when SiC particles are used. Although SiC particles stabilise aluminium foams efficiently, they make the resulting foam brittle, difficult to machine and the manufacture of composites is also expensive<sup>[1]</sup>. Particle-containing alloys can be foamed either by direct gas injection into melts (sometimes called the ‘Alcan route’)<sup>[6,7]</sup> or by ‘foaming of reinforced metals by gas release in precursors’, known under the acronym ‘Formgrip’<sup>[8]</sup>. Recent investigations of foam stabilization suggest that smaller particles (sub- $\mu\text{m}$ -sized) with lower volume fractions, than used in Alcan<sup>[6,7]</sup> or Formgrip processes<sup>[8]</sup> could provide sufficient stability too<sup>[9]</sup>. Dispersing SiC particles in aluminium melts is difficult and expensive<sup>[10]</sup>, especially when the particles are very small. Instead of adding particles from outside, TiC and TiB<sub>2</sub> particles were recently synthesised *in-situ* in a Al-Si melt and were shown to provide good foam stability<sup>[11]</sup>. However the higher processing costs and the toxic gas produced during that synthesis made the processing route questionable. In addition, the thermal instability of TiC and the agglomeration tendency of TiB<sub>2</sub> particles in the melt did not yield consistent foaming properties.

Recently developed aluminium composites containing fine MgAl<sub>2</sub>O<sub>4</sub> particles<sup>[12-14]</sup> appear to be a promising alternative system. MgAl<sub>2</sub>O<sub>4</sub> (spinel) is a reaction product that forms during the reaction of Mg with oxides such as SiO<sub>2</sub> or Al<sub>2</sub>O<sub>3</sub> in aluminium matrix composites<sup>[15]</sup>. Owing to its good wetting with aluminium alloy melt and its good thermal stability, MgAl<sub>2</sub>O<sub>4</sub> has found a place as a reinforcement component in Al composites. An additional advantage is that the particles can be formed *in-situ* by a reaction of oxides with a molten Al-Mg alloy. Unlike the process used for producing TiC and TiB<sub>2</sub> particles, the process of generating solid MgAl<sub>2</sub>O<sub>4</sub> in Al by *in-situ* synthesis is simple, inexpensive and non-toxic. Among the oxides investigated, SiO<sub>2</sub> was found to be the best oxygen source for *in-situ* synthesis due to its high reactivity with Al<sup>[16]</sup>. Still, producing Al composite with MgAl<sub>2</sub>O<sub>4</sub> alone is not straight forward. In an Al matrix MgAl<sub>2</sub>O<sub>4</sub> is always accompanied by

MgO and other transition phases. Process parameters such as Mg concentration, SiO<sub>2</sub> particles size (oxygen source), reaction temperature and reaction time decide which phases are formed.

To develop a suitable material for foaming, some of these parameters were varied in the present study. Only the SiO<sub>2</sub> concentration (5 wt.%) and the reaction temperature (750 °C) were kept to values taken from the literature<sup>[14]</sup>. The composites were reacted for 1, 3 and 5 h only, because beyond 5 h the reaction of SiO<sub>2</sub> with molten Al-Mg alloy slows down or ceases. Synthesising MgAl<sub>2</sub>O<sub>4</sub> *in-situ* in Al alloy melts is now understood but tailoring the microstructural quality in the composite to make it suitable for foaming is a challenge. This ‘quality’ means well-distributed MgAl<sub>2</sub>O<sub>4</sub> particles and the absence of MgO or transition phases (Mg-Al-O, Mg-Al-O-Si and Al-Mg-O) in the matrix. We succeeded to produce a Al/MgAl<sub>2</sub>O<sub>4</sub> composite having this quality and could produce foams comparable to traditional foams like Alporas foams<sup>[1]</sup> or AlSiMg/SiCp metal matrix composites foams produced by formgrip method<sup>[8]</sup>.

## 2. Experimental

### 2.1 Composite synthesis

Al-Mg alloy and 5 wt.% SiO<sub>2</sub> (Quartz or Microsilica) were used as the matrix and reaction agent, respectively. First, Al-Mg alloys of varying Mg content (1–5 wt.%) based on Al of 99.9% purity and Mg of 99.9% purity were prepared in a furnace. SiO<sub>2</sub> was added to the Al-Mg melt by stir casting at the rate of 0.5 wt.% per minute through the vortex created by stirring the molten matrix alloy. The melt was further held for different durations (1 h to 5 h) at 750 °C (1023 K) before casting it in a permanent steel mould. The composites obtained were characterized by X-ray diffraction (XRD), scanning electron microscopy (SEM), energy dispersive spectroscopy (EDS) and optical emission spectroscopy (OES), the latter to

determine the chemical composition. The details of the synthesis and the elemental concentration measured in the composites are given in [Table 1](#).

## 2.2 *Foaming process*

TiH<sub>2</sub> was used as a gas source in all the foaming experiments. The hydride was admixed to the remelted composites containing spinel. Two cases were considered: the melt was left at the foaming temperature to allow the hydride to release gas and create foam without interruption ([see 2.2.1](#)), or the melt was solidified after hydride addition and foaming was carried out in a separate step after this interruption ([see 2.2.2](#)).

### 2.2.1 *Uninterrupted foaming*

In this method, 30 g to 50 g of composites was melted in an alumina crucible in a resistive heating furnace at 700 °C (973 K). After the melt had reached the desired temperature, 1.5 wt.% of untreated TiH<sub>2</sub> powder was admixed to the melt using a graphite stirrer rotating at 600 rpm for 100 s. After mixing, the melt was allowed to foam for further 50 to 200 s inside the furnace, after which the sample was taken out and allowed to solidify via air cooling. The advantage of using untreated TiH<sub>2</sub> is the rapid gas evolution immediate after its addition into the melt, which facilitates a fast foaming process. Both mixing and foaming parameters were based on already optimized values found in the literature<sup>[11,17]</sup>. Uninterrupted foaming as carried out here is similar to what is called the ‘Alporas’ process in the literature with the difference of the foamable melt used<sup>[1]</sup>.

### 2.2.2 *Interrupted foaming*

Interrupted foaming is analogous to what is called the ‘Formgrip’ method in the literature<sup>[8]</sup>. This method consists of two stages in the preparation of foams. In the first stage,

100 g of composite was melted in an alumina crucible inside a furnace at 700 °C. After the melt had reached the desired temperature, 1.5 wt.% of treated TiH<sub>2</sub> powder (pre-oxidized in air for 3 h at 480 °C) was admixed and stirred for 60 s with a graphite stirrer rotating at 600 rpm. Immediately after mixing, the melt was rapidly quenched by pouring it into a water-cooled copper mould of 25 mm diameter and 100 mm height to obtain high density castings. In the second step, these castings were sliced in the transverse direction to obtain the desired size of the foamable precursor. The advantage of using a treated TiH<sub>2</sub> is their surface oxide layer, which slows down the decomposition rate of metal hydride during foam processing and therefore helps in the effective preparation of foamable precursors. Foaming was done by placing precursors in open (25 mm diameter, 150 mm height) or closed (35 mm diameter, 50 mm height) stainless steel moulds, which were heated to the foaming temperatures in a furnace. Further details describing the foaming experiments are given in [Table 2](#). The cross sections of the resulting foams were metallographically polished for macro and microstructural analysis.

### 2.3 X-ray tomography

X-ray tomography of the foams was performed by rotating them through 360° in steps of 1° while acquiring X-ray radiographic images after each step. A description of the X-ray tomographic setup and its operation is reported elsewhere <sup>[1,18]</sup>. Three-dimensional (3D) reconstruction of the data was carried out using the commercial software ‘Octopus’. After reconstruction, the commercial software ‘VGStudioMax 1.2.1’ was used to extract 2D and 3D sections of the foam. The 2D cell area distribution and circularity for selected foams was calculated by analyzing the reconstructed tomographic slices taken from the central part of the foams. This analysis was performed by using the software ‘ImageJ 1.35j’. The porosity of

the foams was measured by 'VGStudioMax 2.0.5' by adjusting the threshold manually for the tomographic slices.

### 3. Results

#### 3.1 Composite synthesis

Figure 1 shows SEM micrographs of composite 1c, produced at 750°C for 5 h. The composite contains fine  $\text{MgAl}_2\text{O}_4$  particles of octahedral morphology and blocky Mg-Al-O transition phases in a Al-Si matrix. Fine Al-Mg-O transition phases along with  $\text{MgAl}_2\text{O}_4$  particles were also found. The results of microscopy are confirmed by the EDX microanalysis of the phases present in the matrix, which is described in the second last paragraph of this section. For this trial, 1 wt.% Mg and quartz particles ( $\text{SiO}_2$ ) of 200  $\mu\text{m}$  size were chosen. Selecting this Mg content was motivated by the fact that  $\text{MgAl}_2\text{O}_4$  is the dominant phase that forms at Mg contents <2wt.% [16,19]. The choice of  $\text{SiO}_2$  particle size aims at creating larger nucleation sites for  $\text{MgAl}_2\text{O}_4$  by reactive wetting of Al and Mg.  $\text{MgAl}_2\text{O}_4$  particles form after even shorter reaction time (1 h) for composite 1. Only a small increase of volume is evident after 5 h of holding, even though 97% of Mg and 88% of  $\text{SiO}_2$  are consumed during the reaction.

Figure 2 shows SEM micrographs of composite 2c, also produced at 750°C for 5 h. The microstructure exhibits agglomerated  $\text{MgAl}_2\text{O}_4$  particles along with Al-Mg-O phases and Mg-Al-O transition phases in an Al-Si matrix. Decreasing the quartz ( $\text{SiO}_2$ ) particle size to 100  $\mu\text{m}$  and increasing the Mg concentration to 5 wt.% does not improve the extent of reaction in comparison to composite 1, see Table 1, but the higher Mg content facilitates  $\text{MgAl}_2\text{O}_4$  formation in larger quantity compared to composite 1. During the initial hours of reaction, the dominant phase formed is MgO, since the Mg concentration is >2wt.% [16,19]. On even longer holding, MgO converts into  $\text{MgAl}_2\text{O}_4$  through Mg-Al-O-Si and Mg-Al-O

transition phases, but some MgO persists even after 5 h of holding due to the higher Mg concentration (5 wt.%) used in this trial. The  $\text{MgAl}_2\text{O}_4$  particles are mostly found accumulated at the reaction site and cannot be separated from each other even by stirring the melt.

The SEM micrographs of composite 3 (Figure 3) produced at  $750^\circ\text{C}$  for 5 h shows ultra-fine octahedral  $\text{MgAl}_2\text{O}_4$  crystals (80 nm to 2  $\mu\text{m}$ ) well distributed in the Al-Si matrix. In this trial, microsilica particles ( $\text{SiO}_2$ ) of 44  $\mu\text{m}$  size were chosen instead of the coarse quartz particles used for trials 1 and 2. The Mg concentration is adjusted to 2.6 wt.% to largely suppress the formation of MgO. The advantage of microsilica particles is that they are porous, i.e. each particle is an assembly of sub- $\mu\text{m}$ -sized silica spheres. Because of the porous structure the availability of an interface between  $\text{SiO}_2$  and molten Al-Mg increases, which in turn increases the extent of reaction.

Energy dispersive X-ray spectra (EDS) of different phases present in the composites are given in Figure 4. Their corresponding quantitative elemental analysis is listed in Table 3. The identity of  $\text{MgAl}_2\text{O}_4$ , generally observed as octahedral crystals by SEM, can be confirmed with EDS by calculating the Al/Mg ratio, which is equal to 2 for stoichiometric spinel i.e.,  $\text{MgAl}_2\text{O}_4$  (the oxygen composition from EDS can be ignored). EDS analyses have identified Mg and Al in the blocky particles (Mg-Al-O transition phase), where the Al/Mg ratio is found to be 2.14 (Table 3). In this study, the phases containing Al, Mg, O and Si with varying atomic fractions have also been identified in composite 2. They must be classified as a Mg-Al-O-Si transition phase existing between MgO and  $\text{MgAl}_2\text{O}_4$ . Although the Al/Mg ratio of these phases can fall anywhere between 0 and 2 (0 for MgO), Table 3 only lists values from 0.35 to 1.48. Similarly, the fine cubic phases (some are isolated, see Figure 1b, and some are adhering to  $\text{MgAl}_2\text{O}_4$ , see Figure 2b) containing different atomic fractions of Al, Mg, and O found in all the composite samples are considered as Al-Mg-O transition

phases between  $\text{MgAl}_2\text{O}_4$  and  $\text{Al}_2\text{O}_3$  that are formed during disintegration of  $\text{MgAl}_2\text{O}_4$ . These are rich in Al and the Al/Mg ratio falls between 3 and 14 (Table 3). EDS for MgO was difficult to carry out due to their fineness. Figure 5 shows the XRD patterns of composites 2c and 3, both obtained after 5 h of reaction at  $750^\circ\text{C}$ .  $\text{MgAl}_2\text{O}_4$  peaks can be observed in both the composites. In addition to  $\text{MgAl}_2\text{O}_4$ , peaks obtained for composite 2c confirm the presence of MgO,  $\text{SiO}_2$  and other transition phases in the matrix alloy.

The degree of  $\text{SiO}_2$  reaction and Mg consumption is estimated from the Si and Mg concentration measured using OES on bulk composites obtained after different reaction times. If  $\text{SiO}_2$  reacted completely, it would release 2.34 wt.% of Si to the molten Al<sup>[14]</sup>. From Table 1 it is understood that composite 3 exhibits a higher extent of reaction in comparison to composites 1 and 2 after 5 h of holding. However a complete reaction is not achieved for any of the composites. The volume fraction of  $\text{MgAl}_2\text{O}_4$  particles in composite 3 can be estimated using the actual composition of Si and Mg measured, which is 3.4 vol.%.

### 3.2 Foaming Process

Figure 6 shows cross sectional macrographs of foams made from composites 1c, 2a, 2c, and 3. The foams are produced through uninterrupted foaming (Table 2). The composites chosen for foaming reacted for 5 h except for composite 2a which was reacted for 1 h only. Obviously, geometrical features such as cell shape, cell size and cell size distribution of the foams vary for the different composites. The composite 1c foam exhibits irregular cell shape and size distribution with a liquid sump at the bottom, indicating drainage. The overall structure of the composite 2a foam is poor with no definite cell shape. Composite 2c foam exhibits spherical cavities embedded in the metallic matrix, suggesting that this foam lacked in expansion. Finally, composite 3 foam exhibits the most regular cell shape and the most uniform cell size distribution among all the foams produced. In addition, the expansion of



composite 3 foam is higher than that of the other foams, when considering the initial weight (g) of the precursors, see [Table 2](#). The 2D cell circularity of the foams is analyzed in order to differentiate their structural quality. The circularity  $C$  of a cell is defined as  $4\pi A/P^2$ , where  $A$  and  $P$  are the area and perimeter of the cell. If  $C$  approaches 1, the cell resembles a circle. The details of the analysis are reported in Ref. [18](#). [Figure 7](#) shows the circularity vs. equivalent diameter for the various composite foams. All foams show a significant difference in the cell circularity. Among the foams, composite 3 foam exhibits the most polyhedrally shaped cells among the large number of small cells.

Based on the comparisons between different composites, the expansion and stability of composite 3 foams as a function of time was investigated through interrupted foaming ([Table 2](#)). [Figure 8](#) shows 2D and 3D X-ray tomographic reconstructions of transverse and longitudinal sections of composite 3 foams baked in a closed steel mould at 675 °C for either 300 s or 480 s. The foaming temperature is kept low in this case of uninterrupted foaming in order to avoid rapid gas evolution. The diameter of the precursor is 25 mm which is smaller than the mould diameter (35 mm). Hence the foam expands in both the transverse and longitudinal directions. The resulting foams exhibit a regular cell shape and uniform size distribution throughout the cross section. Due to the lower foaming temperature the expansion is slow and continues even after 300 s. Only after 480 s the foam shows a polyhedral cell shape with thin cell walls and a uniform cell size distribution. The porosity measured using image analysis technique is 0.74 for 300 s and 0.80 for 480 s foaming time.

[Figure 9](#) shows 3D X-ray tomographic reconstructions of longitudinal cross sections of composite 3 foams baked in an open steel mould at 740°C for 100 s and 150 s. In this case, the foams were allowed to expand only unidirectionally as the mould and the precursor diameters were the same. The expansion is faster due to the higher foaming temperature compared to foaming in the closed moulds. The macrostructure of the foam in [Figure 9a](#)

contains small cells evenly distributed throughout the cross section and a few larger cells at the top. In [Figure 9b](#) the cells have expanded to an equiaxed shape with significant cell wall thinning. No drainage is observed in both cases. The 2D cell size distribution of the foams based on the area fraction is shown in [Figure 10](#). The area fraction is defined as the area contribution of a cell size class related to the total area of all the cells <sup>[18]</sup>. In our case, the distribution is more uniform for 100 s of foaming than for 150 s. Log-normal fitting of the distributions provides a mean cell diameter  $D_{\text{mean}}$  for both the foams, which is  $1.53 \pm 0.48$  mm for 100 s foaming time and  $2.85 \pm 0.49$  mm for 150 s. The porosity measured is 0.67 and 0.75 for 100 s and 150 s, respectively. Foam expansion could be determined with respect to the volume of the original precursors since foaming was unidirectional. The measured values are 300% and 400% expansion for 100 s and 150 s of foaming, respectively.

### 3.3 Foam microstructures

A cell wall cross section of composite 2c foam is visualised by SEM in [Figure 11](#) and shows  $\text{MgAl}_2\text{O}_4$  agglomerates and Mg-Al-O particles, both  $\approx 100$   $\mu\text{m}$  in size. The cell surface contains MgO, Mg-Al-O-Si and few  $\text{MgAl}_2\text{O}_4$  particles (octahedral crystals). The  $\text{MgAl}_2\text{O}_4$  particles seen in the cell surface are basically a corner of an agglomerate protruding out of the side of the cell wall. Hence they appear to be not embedded in the surface. The cell wall cross sections of composite 3 foam in [Figure 12](#) exhibit a large volume fraction of fine  $\text{MgAl}_2\text{O}_4$  particles. The particle arrangement on the cell walls is hard to characterise due to difficulties in preserving the edges during polishing.

## 4. Discussion

### 4.1 Composite synthesis

The experiments clearly showed that among the three different composites produced, composite 3 that was obtained after 5 h of reaction has the microstructure that leads to effective foaming (The resulting foams show better cell shape, uniform cell size distribution and zero drainage). It contains small  $\text{MgAl}_2\text{O}_4$  particles that are uniformly distributed in the matrix alloy and only few transition phases. The key for this success was the use of microsilica ( $\text{SiO}_2$ ) particles as an oxygen source and the proper adjustment of the Mg concentration. In  $\text{SiO}_2$  containing molten Al-Mg alloy, Mg segregates on  $\text{SiO}_2$  and reduces the interfacial energy, which promotes the initial wetting and subsequently the reaction between Al and  $\text{SiO}_2$ .

From the displacement reactions of  $\text{SiO}_2$  in Al-Mg alloy reported in Ref.20, it is understood that the amount of  $\text{SiO}_2$  consumed for the formation of MgO is less compared to the formation of  $\text{MgAl}_2\text{O}_4$ . Therefore, a continuous reaction between  $\text{SiO}_2$  and Al-Mg alloy melt at the interface (or interfacial diffusion) is essential for the formation of  $\text{MgAl}_2\text{O}_4$  or MgO to  $\text{MgAl}_2\text{O}_4$  transformation. If larger particles are chosen, e.g. quartz powder of 200  $\mu\text{m}$  or 100  $\mu\text{m}$  grain size, the extent of reaction between  $\text{SiO}_2$  and molten Al-Mg is reduced with longer holding time, which is evident from the elemental concentration of Si and Mg measured in the bulk composite, see Table 1. The accumulation of reaction products at the reaction sites limits solid state diffusion of the reactive elements Mg and Al through the reaction product layer. In composite 3, the degree of reaction has been improved due to the porous structure of the microsilica used as well as its small mean particles size (44  $\mu\text{m}$ ), which provides silica surfaces for a continuous reaction to form  $\text{MgAl}_2\text{O}_4$  or to transform MgO to  $\text{MgAl}_2\text{O}_4$ .

The optimum Mg content required for a complete reaction is not known. The lower Mg concentration (1 wt.%) used in the first trial did not yield a sufficient quantity of  $\text{MgAl}_2\text{O}_4$  particles even after 5 h of holding and the composite contained blocky Mg-Al-O transition phases. The conversion of Mg-Al-O to  $\text{MgAl}_2\text{O}_4$  depends on Mg and Al diffusion, which slows down on longer holding due to insufficient Mg concentration. Increasing the Mg concentration to 5wt.% yielded a larger volume of  $\text{MgAl}_2\text{O}_4$ , but only after longer holding. When the concentration of Mg in Al is  $>2$  wt.%, sub- $\mu\text{m}$ -sized MgO forms as a dominant phase within the first hour of reaction<sup>[19]</sup>. On longer holding, MgO converts into  $\text{MgAl}_2\text{O}_4$ , through Mg-Al-O-Si and Mg-Al-O transition phases. Since  $>4$  wt.% of Mg are added in composite 2, some MgO persists even after longer holding as it is understood from the literature<sup>[19]</sup>. It is likely that some MgO is also present in composite 3, but in such low concentration that it could not be detected using X-ray diffraction or electron microscopy. This is attributed to the amount of Mg addition (2.6 wt.%), which is slightly above the MgO persistence limit and/or due to the porous structure of the microsilica particles<sup>[16]</sup>. Therefore, a more detailed investigation of  $\text{MgAl}_2\text{O}_4$  formation kinetics might lead to further improved Al composites reinforced exclusively with  $\text{MgAl}_2\text{O}_4$  particles.

#### 4.2 Foaming

Uninterrupted foaming of all 4 composites (1c, 2a, 2c and 3) produced foams, but the degree of expansion, foam stability and cell structure strongly varied. Composite 3 foam (Figure 6d) exhibited the highest expansion and the most regular cell shape. The blocky Mg-Al-O particles in composites 1c and 2a negatively affected foam expansion and cell shape. The poor structure of composite 2a foam might also be related to a too high melt viscosity caused by the higher content (see Table2) of free Mg, which during stirring and admixing of the blowing agent (100 s in this case) reacts with atmospheric oxygen to form MgO<sup>[21]</sup>. An

excess viscous force in the liquid would then prevent the cells from achieving an equilibrium shape<sup>[10]</sup>, and introduce some non-uniformity to the cell structure<sup>[22]</sup>. It is noteworthy that composite 2a contains sub- $\mu\text{m}$ -sized MgO particles in addition to the blocky Mg-Al-O phases. MgO particles are equally wettable by Al as  $\text{MgAl}_2\text{O}_4$ . However, their needle-like morphology and presence as agglomerates in the matrix does not allow them to act as particle stabilizers. Composite 2c also contains same free Mg (2.69 wt.%) and therefore also influences melt viscosity as for composite 2a. Its foam structure is very stable due to the presence of  $\text{MgAl}_2\text{O}_4$ , but the foam lacks in expansion due to  $\text{MgAl}_2\text{O}_4$  agglomerates and blocky Mg-Al-O phases. Even stirring during admixing  $\text{TiH}_2$  cannot sufficiently distribute the  $\text{MgAl}_2\text{O}_4$  particles in the melt. Composite 3 itself contains 1.26 wt.% Mg excess compared to the  $\text{MgAl}_2\text{O}_4$  stoichiometry. The viscosity of the melt is higher even in this case, however not as high as for composite 2a and 2c.

Interrupted foaming has many advantages in comparison to other foaming techniques<sup>[8]</sup>. The shorter stirring time (60 s) required for admixing the blowing agent limits the undesirable increase of melt viscosity. The equiaxed cell shape and thinner cell walls and the absence of fine cavities in the corresponding composite 3 foams show this. Foaming could be further improved by lowering the foaming temperature to lower values than applied in the present study for a more controlled gas evolution without compromising on melt fluidity. This could be achieved by creating  $\text{MgAl}_2\text{O}_4$  particles in a AlSi alloy matrix contains  $\geq 9\text{wt}\%$  Si.

The wettability of a particle is understood to have an essential influence on foam stabilization<sup>[23–25]</sup>. An optimum wetting angle range of  $75^\circ$ – $85^\circ$  for particles has been determined experimentally by Sun and Gao<sup>[26]</sup>. They also found stable foam for wetting angles above  $90^\circ$ , in which case the particles are strongly attached to the gas solid interface. This contradicts models by Kaptay<sup>[27]</sup>, who predicted that no foam stability is possible from  $20^\circ$  to  $90^\circ$  wetting angle.  $\text{MgAl}_2\text{O}_4$  is an interfacial product with an improved wettability by

liquid Al <sup>[7,15,28]</sup> and has been used for Al foam stabilization for the first time in the present study. The suitability of MgAl<sub>2</sub>O<sub>4</sub> has been derived from the wettability of SiC in commercial Al composites used for foaming. In general, those alloys contain Mg which improves the wettability of the SiC particles that contain 0.1-0.2 wt.% of SiO<sub>2</sub> in form of a surface layer already when they are added to the melt <sup>[15]</sup>. SiO<sub>2</sub> has a poor wettability (contact angle 120°) with molten Al at 700°C <sup>[16]</sup> but as Mg reacts with SiO<sub>2</sub> and forms MgO or MgAl<sub>2</sub>O<sub>4</sub> (depending upon the Mg concentration), wetting is improved at the interface between SiC and Al. An analogous effect has been observed by researchers investigating the effect of Mg on Al foams stabilized by Al<sub>2</sub>O<sub>3</sub> particles <sup>[29]</sup>.

The wetting angle of MgAl<sub>2</sub>O<sub>4</sub> with Al is unknown. Klinger et al <sup>[30]</sup> have shown that at 700°C the wetting angle of Al<sub>2</sub>O<sub>3</sub> particle with AlMg1 alloy is 90°. At this temperature and Mg concentration, 1 µm thickness MgAl<sub>2</sub>O<sub>4</sub> crystals form on the Al<sub>2</sub>O<sub>3</sub> particles as an interfacial product <sup>[15]</sup>. From the cell surface topography (Figure 10) it is clear that the MgAl<sub>2</sub>O<sub>4</sub> particles are at the gas/solid interface and are embedded in the cell wall materials, which could point at a wetting angle of MgAl<sub>2</sub>O<sub>4</sub> particle around 90°. Particle pushing effects during solidification shall be ignored in this case. The fcc crystal structure and the lattice mismatch of 0.25% between MgAl<sub>2</sub>O<sub>4</sub> (100) and Al (100) plane is one of the lowest among all reinforcements <sup>[31]</sup> and would allow the particle to act as a nucleation site for α-Al. Therefore MgAl<sub>2</sub>O<sub>4</sub> particles are likely to remain at the grain centres instead of being pushed to the grain boundaries by the growing Al solid.

Considering the presence of MgAl<sub>2</sub>O<sub>4</sub> at the cell surface and the absence of particles inside the cell walls, it is valid to assume that the particle arrangement at the gas solid interfaces is as sketched schematically in Figure 13. Due to the small size of our MgAl<sub>2</sub>O<sub>4</sub> particles, a full coverage of the entire cell surface can be achieved despite the low volume fraction of 3.4%. This is far less than the SiC contents used in commercial foamable

composites (10% or more) and emphasizes the possibility of using smaller particles for foam stabilization.

## 5. Conclusions

1. Our trial experiments have led to the development of a novel foamable Al alloy containing some volume percent of small  $\text{MgAl}_2\text{O}_4$  particles.
2. The microstructural quality of the precursor has a crucial influence on foaming. The uniformity of  $\text{MgAl}_2\text{O}_4$  particle distribution in the matrix and the absence of transition phases are essential.
3. Fine needle like MgO particles are also present in both composite 2 and 3 depending on their free Mg concentration excess compared to the  $\text{MgAl}_2\text{O}_4$  stoichiometry. MgO particles are equally wettable by Al as  $\text{MgAl}_2\text{O}_4$ . However, their needle-like morphology and presence as agglomerates in the matrix does not allow them to act as a particle stabilizer.
4. Ultra-fine octahedral  $\text{MgAl}_2\text{O}_4$  crystals can act as a stabilizing agent for Al alloy foam. Their wetting angle with Al is unknown. However, the cell surface topography after solidification suggests that  $\text{MgAl}_2\text{O}_4$  particles are partially wetted by Al.
5. The present study underlines the better possibility of using smaller particles for foam stabilization. Composite 3 foam that exhibits the best stability and expansion contains only 3.4 vol.% of  $\text{MgAl}_2\text{O}_4$  particles for stabilization.

## References

1. J. Banhart: *Prog. Mater. Sci.*, 2001, vol. 46, pp. 559–632.
2. S.W. Ip, Y. Wang, and Y. Toguri JM: *Can. Metall. Quart.*, 1999, vol. 38, pp. 81–92.
3. J. Banhart: *J. Met.*, 2000, vol. 52, pp. 22–27.
4. N. Babcsán, D. Leitlmeier, and H.-P. Degischer: *Mat.-wiss. u. Werkstofftech.*, 2003, vol. 34, pp. 22–29.
5. G. Kaptay, in *Advanced Metallic Materials*, J. Jerz, P. Šebo, M. Zemánková, eds, Slovak Academy of Sciences, Bratislava, Slovakia, 2003, pp. 22-29.
6. D. Leitlmeier, H.P. Degischer, and H.J. Flankl: *Adv. Eng. Mater.*, 2004, vol. 4, pp. 735–740.
7. N. Babcsán, D. Leitlmeier, H.P. Degischer, and J. Banhart: *Adv. Eng. Mater.*, 2004, vol. 6, pp. 421–428.
8. V. Gergely and B. Clyne: *Adv. Eng. Mater.*, 2000, vol. 2, pp. 175–178.
9. A. Haibel, A. Rack, and J. Banhart: *Appl. Phys. Lett.*, 2006, vol. 89, 154102.
10. O. Prakash, H. Sang, and J.D. Embury: *Mater. Sci. Eng. A*, 1995, vol. 199, pp. 195–203.
11. N. Babcsán, G. S. Vinod Kumar, B. S. Murty, and J. Banhart: *Trans. Indian Inst. Met.*, 2007, vol. 60, pp. 127-132.
12. P.C. Maity, P.N. Chakraborty, and S.C. Panigrahi: *Mater. Lett.*, 1994, vol. 20, pp. 93–97.
13. P.C. Maity, P.N. Chakraborty, and S.C. Panigrahi: *J. Mater. Sci.*, 1996, vol. 31, pp. 6377–6382.
14. V. M. Sreekumar, Ph.D thesis, Indian Institute of Technology, Kharagpur 2008.
15. B.C. Pai, G. Ramani, R. M. Pillai, and K.G. Satyanarayana: *J. Mater. Sci.*, 1995, vol. 30, pp. 1903–1911
16. V. M. Sreekumar, R. M. Pillai, B.C. Pai, and M. Chakraborty: *Appl. Phys. A*, 2008, vol. 90, pp. 745–752.
17. Z-L. Song, J-S. Zhu, L-Q. Ma, and D-P. He: *Mater. Sci. Eng. A*, 2001, vol. 298, pp. 137–143.



18. M. Mukherjee, U. Ramamurty, F. Garcia-Moreno, and J. Banhart: *Acta Mater.*, 2010, vol. 58, pp. 5031–5042.
19. Z. Shi, S. Ochiai, M. Gu, M. Hojo, and J.C. Lee: *Appl. Phys. A*, 2002, vol. 74, pp. 97–10
20. V.M. Sreekumar, K.R. Ravi, R.M. Pillai, B.C. Pai, and M. Chakraborty, *Met. Mater. Trans. A*, 2008, vol.39, pp.919-933
21. S.Y. Kim, Y.S. Um, and B.Y. Hur: *Mater. Sci. Forum.*, 2006, vol. 510–511, pp. 902–905.
22. C.C. Yang and H. Nakae: *J. Mater. Process. Tech.*, 2003, vol. 141, pp. 202–206.
23. A. Dippenaar: *Int. J. Miner. Proc.*, 1982, vol. 9, pp. 1–14.
24. B. P Binks: *Curr. Opin. Colloid Interface Sci.*, 2002, vol. 7, pp. 21– 41.
25. G. Johansson and R. Pugh: *Int. J. Mineral Process.*, 1992, vol. 34, pp. 1–21
26. Y.Q. Sun and T. Gao: *Met. Mater. Trans. A*, 2002, vol. 33, pp. 3286–3292.
27. G. Kaptay: *Colloids Surf A: Physicochem. Eng. Aspects*, 2006, 282–283, pp. 387–401.
28. V. Gergely, D.C. Curran, and T.W. Clyne: *Comp. Sci. Tech.*, 2003, vol. 63, pp. 2301–2310.
29. S. Asavavisithchai and A.R. Kennedy: *Scr. Mater.*, 2006, vol. 54, pp. 1331–1334
30. A. J. Klinter, C. A. Leon, and R. A. L. Drew: *J. Mater. Sci.*, 2010, vol. 45, pp. 2174–2180.
31. S. B. Sinnott and E. C. Dickey: *Mater. Sci. & Engg. R*, 2003, vol. 43, pp. 1–59.

## Figure Captions

- Fig.1 SEM micrographs of composite 1c (Al-1Mg-5SiO<sub>2</sub>) reacted at 750°C for 5 h with quartz powder of mean particle size of 200 μm serving as oxygen source. Blocky Mg-Al-O (transition phase), fine MgAl<sub>2</sub>O<sub>4</sub> particles of octahedral morphology (grey colour) and Al-Mg-O (transition phase) are shown in two images of different magnification.
- Fig.2 SEM micrographs of composite 2c (Al-5Mg-5SiO<sub>2</sub>) reacted at 750°C for 5 hours with quartz powder of mean particle size of 100 μm serving as oxygen source. (a) Features particles agglomeration and Mg-Al-O transition phase. (b) MgAl<sub>2</sub>O<sub>4</sub> particles and Al-Mg-O are seen in higher magnification.
- Fig.3 SEM micrographs of composite 3 (Al-2.6Mg-5SiO<sub>2</sub>) reacted at 750°C for 5 hours with micro silica powder of 44 μm particle size serving as oxygen source. Many octahedral MgAl<sub>2</sub>O<sub>4</sub> particles and few Al-Mg-O particles embedded in the aluminium matrix, but neither MgO nor Mg-Al-O phases occur.
- Fig.4 EDX spectra of phases present in the bulk of composites 1, 2 and 3. (a) Mg-Al-O-Si (Al/Mg = 0.35), (b) Mg-Al-O-Si (Al/Mg = 1.48), (c) Mg-Al-O (Al/Mg = 2.14), (d) MgAl<sub>2</sub>O<sub>4</sub> (Al/Mg = 2.02), (e) Al-Mg-O (Al/Mg = 13.72), Table 3 gives the composition of the phases in at.% as measured using EDX. The intense Al peak observed in the spectrum possibly includes contributions of the Al matrix due to the small particles size.

Fig.5 X-ray diffraction patterns showing the presence of Al, Si,  $MgAl_2O_4$ , in composites 2c and 3. Composite 2c also shows the presence of MgO,  $SiO_2$  and transition phases.

Fig.6 Cross sectional macrographs of foams produced using (a) composite 1c (b) composite 2a (c) composite 2c and (d) composite 3. The foams were made through uninterrupted foaming using untreated  $TiH_2$ , mixing time 100s, holding time 200s. The details of foaming are given in Table 2.

Fig.7 Circularity vs. equivalent diameter of the cells in the foams made from (a) composite 1a, (b) composite 2a (c) composite 2c and (d) composite 3.

Fig.8 2D and 3D X-ray tomographic reconstruction of transverse and longitudinal sections of composite 3 foams baked in a closed steel mould at  $675^\circ C$  (40 mm diameter and 50 mm height). (a) baking time 300 s, porosity  $\approx 0.74$  (b) baking time 480 s, porosity  $\approx 0.80$ .

Fig.9 3D X-ray tomographic reconstruction of longitudinal cross section of composite 3 foams baked in an open steel mould at  $740^\circ C$  (25mm diameter and 150 mm height). (a) baking time 100 s, porosity  $\approx 0.67$  and, (b) baking time 150 s, porosity  $\approx 0.75$ . The top dome of the second foam was destroyed during blowing air for solidification. The volume expansion of the foams obtained after 100 s and 150 s with respect to the original precursor volume is 3 times and 4 times, respectively.

Fig.10 2D cell size distribution for composite-3 foams baked in an open steel mould (25mm diameter and 150 mm height) at  $740^\circ C$  for, (a) 100 s (b) 150 s.

Fig.11 SEM micrographs of the cross section of cells of composite 2c foam. (a) Cross section of a cell wall, (b) inner cell surface covered with Mg-Al-O-Si and few  $MgAl_2O_4$  particles, (c) higher magnification revealing particles on the inner cell surface, (d) another region of cell surface showing fine needle-shaped MgO particles and spherical Mg-Al-O-Si phase.

Fig.12 SEM micrographs of the inner surface of cells of composite 3 foam. (a) Cross section of a cell wall and inner cell surface covered with  $MgAl_2O_4$  particles, (b) embedded particles at the cell surface, (c) higher magnification of inner cell surface (d) a  $MgAl_2O_4$  (octahedral crystal) particle on the cell surface. Since these particles are finer it was more difficult to preserve the arrangement of particles at the edge of the cell wall while polishing the cross section.

Fig.13 Idealised schematic of cell wall cross section of composite 2c and composite 3 foams showing the arrangement of the stabilizing particles inside the film and in the gas solid interface.

**Table 1. Details of synthesis of Al-Mg-SiO<sub>2</sub> composite**

Code		Reaction Temperature °C	Reaction time hours	Source composition Wt.%		Measured elemental composition (wt.%) and equivalent reaction of SiO <sub>2</sub> and consumption of Mg due to the reaction (5wt% of Silica releases 2.338wt.% of Si)			
				SiO <sub>2</sub>	Mg	Mg	Si	Mg consumption (%)	SiO <sub>2</sub> reaction (%)
Composite-1	a	750	1	5(quartz (200µm))	1	0.30	1.84	70	73
	b	750	3			0.10	2.01	90	81
	c	750	5			0.03	2.07	97	82
Composite-2	a	750	1	5 (quartz 100µm)	5	2.69	1.73	46	74
	b	750	3			2.67	1.76	46	75
	c	750	5			2.69	1.91	46	81
Composite-3		750	5	5 (micro Silica 44µm)	2.6	1.2	2.2	55	94

**Table 2. Details of foaming tests conducted for the composites**

No.	Precursor	Foaming method	Weight in g	Blowing agent	Stirring Time s	Foaming Temp	Foaming Time s
1	Composite-1c	uninterrupted	53	untreated TiH <sub>2</sub>	100	700	200
2	Composite-2a	uninterrupted	62	untreated TiH <sub>2</sub>	100	700	200
3	Composite-2c	uninterrupted	35	untreated TiH <sub>2</sub>	100	700	200
4	Composite-3	uninterrupted	26	untreated TiH <sub>2</sub>	100	700	200
5	Composite-3	interrupted	22.5	treated TiH <sub>2</sub>	70s	740	100
6	Composite-3	interrupted	22.9	treated TiH <sub>2</sub>	70s	740	150
7	Composite-3	interrupted	22.5	treated TiH <sub>2</sub>	70s	675	300
8	Composite-3	interrupted	23	treated TiH <sub>2</sub>	70s	675	480

**Table 3. EDX bulk elemental analysis of Mg-Al-O-Si, Mg-Al-O, MgAl<sub>2</sub>O<sub>4</sub>, and Al-Mg-O phases**

Elements	Mg-Al-O-Si					Mg-Al-O	MgAl <sub>2</sub> O <sub>4</sub>	Al-Mg-O	
	(at.%)					(at.%)	(at.%)	(at.%)	
<b>O</b>	<b>81.08</b>	<b>81.68</b>	<b>76.89</b>	<b>74.18</b>	<b>74.03</b>	<b>59.38</b>	<b>61.99</b>	<b>55.53</b>	<b>43.26</b>
<b>Mg</b>	<b>10.86</b>	<b>10.26</b>	<b>11.07</b>	<b>10.43</b>	<b>8.63</b>	<b>12.19</b>	<b>12.06</b>	<b>9.33</b>	<b>3.76</b>
<b>Al</b>	<b>3.86</b>	<b>4.90</b>	<b>6.58</b>	<b>10.87</b>	<b>12.83</b>	<b>26.15</b>	<b>24.46</b>	<b>34.55</b>	<b>51.61</b>
<b>Si</b>	<b>1.08</b>	<b>0.18</b>	<b>0.76</b>	<b>0.27</b>	<b>6.82</b>			-	-
<b>Al/Mg</b>	<b>0.35</b>	<b>0.47</b>	<b>0.59</b>	<b>1.04</b>	<b>1.48</b>	<b>2.14</b>	<b>2.02</b>	<b>3.70</b>	<b>13.72</b>

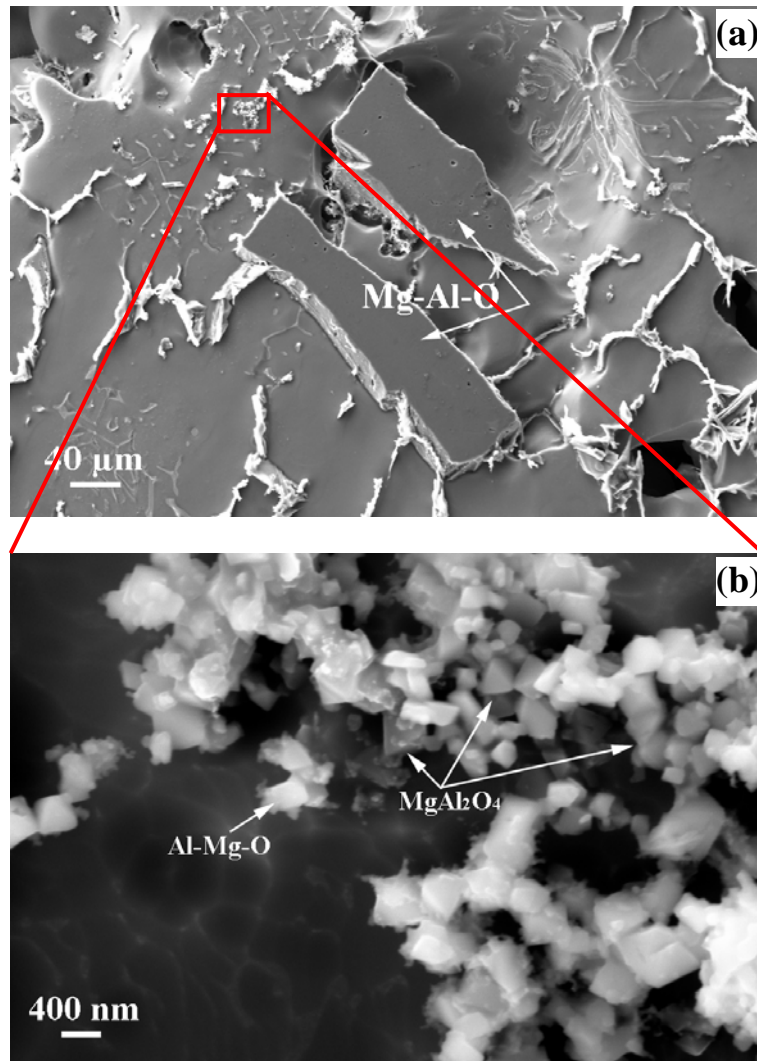


Fig.1 SEM micrographs of composite 1c ( $\text{Al-1Mg-5SiO}_2$ ) reacted at  $750^\circ\text{C}$  for 5 h with quartz powder of mean particle size of  $200\ \mu\text{m}$  serving as oxygen source. Blocky Mg-Al-O (transition phase), fine  $\text{MgAl}_2\text{O}_4$  particles of octahedral morphology (grey colour) and Al-Mg-O (transition phase) are shown in two images of different magnification.

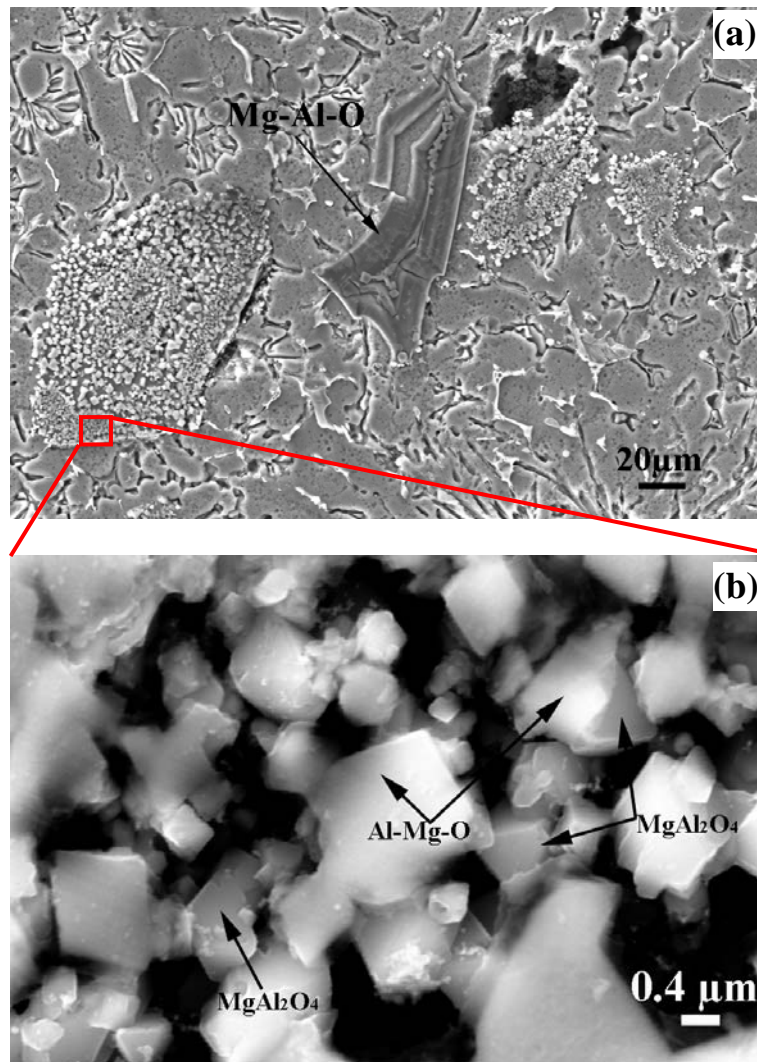


Fig.2 SEM micrographs of composite 2c (Al-5Mg-5SiO<sub>2</sub>) reacted at 750°C for 5 hours with quartz powder of mean particle size of 100 μm serving as oxygen source. (a) Features particles agglomeration and Mg-Al-O transition phase. (b) MgAl<sub>2</sub>O<sub>4</sub> particles and Al-Mg-O are seen in higher magnification.



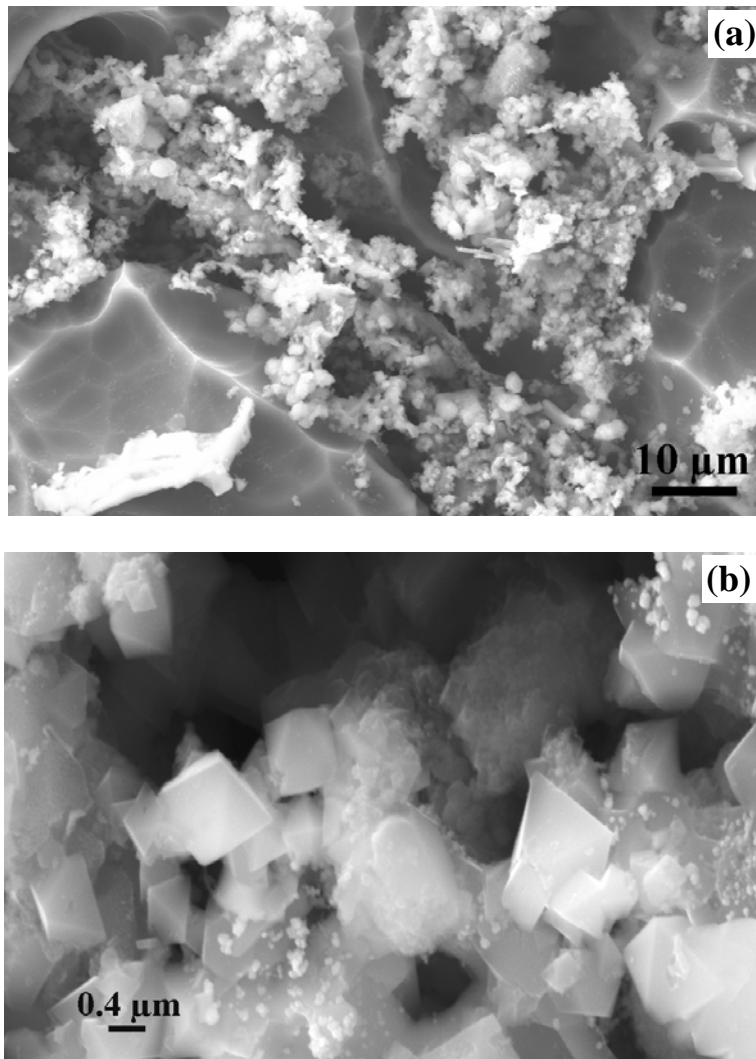


Fig.3 SEM micrographs of composite 3 ( $\text{Al-2.6Mg-5SiO}_2$ ) reacted at  $750^\circ\text{C}$  for 5 hours with micro silica powder of  $44\ \mu\text{m}$  particle size serving as oxygen source. Many octahedral  $\text{MgAl}_2\text{O}_4$  particles and few  $\text{Al-Mg-O}$  particles embedded in the aluminium matrix, but neither  $\text{MgO}$  nor  $\text{Mg-Al-O}$  phases occur.

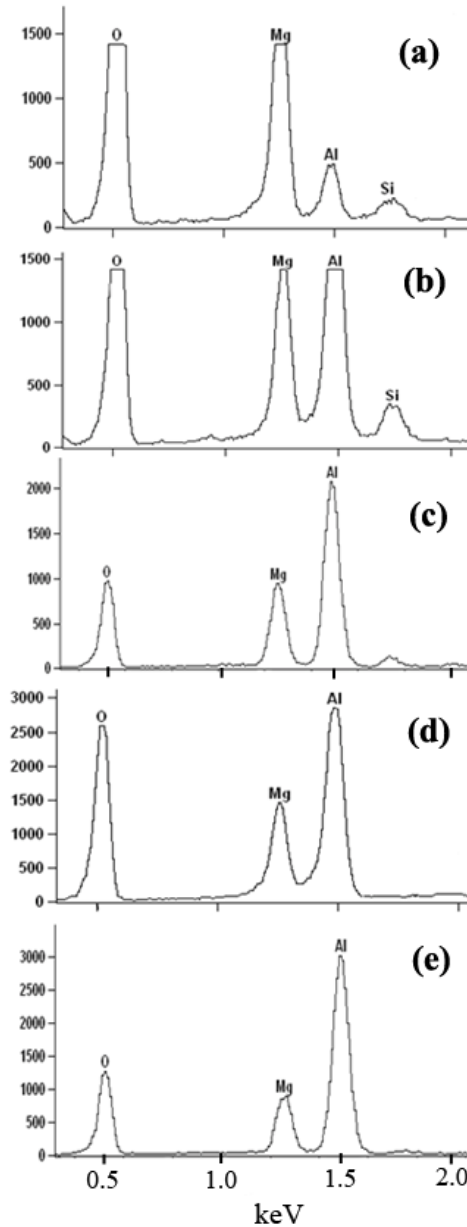


Fig.4 EDX spectra of phases present in the bulk of composites 1, 2 and 3. (a) Mg-Al-O-Si (Al/Mg = 0.35), (b) Mg-Al-O-Si (Al/Mg = 1.48), (c) Mg-Al-O (Al/Mg = 2.14), (d)  $MgAl_2O_4$  (Al/Mg = 2.02), (e) Al-Mg-O (Al/Mg = 13.72), Table 3 gives the composition of the phases in at.% as measured using EDX. The intense Al peak observed in the spectrum possibly includes contributions of the Al matrix due to the small particles size.

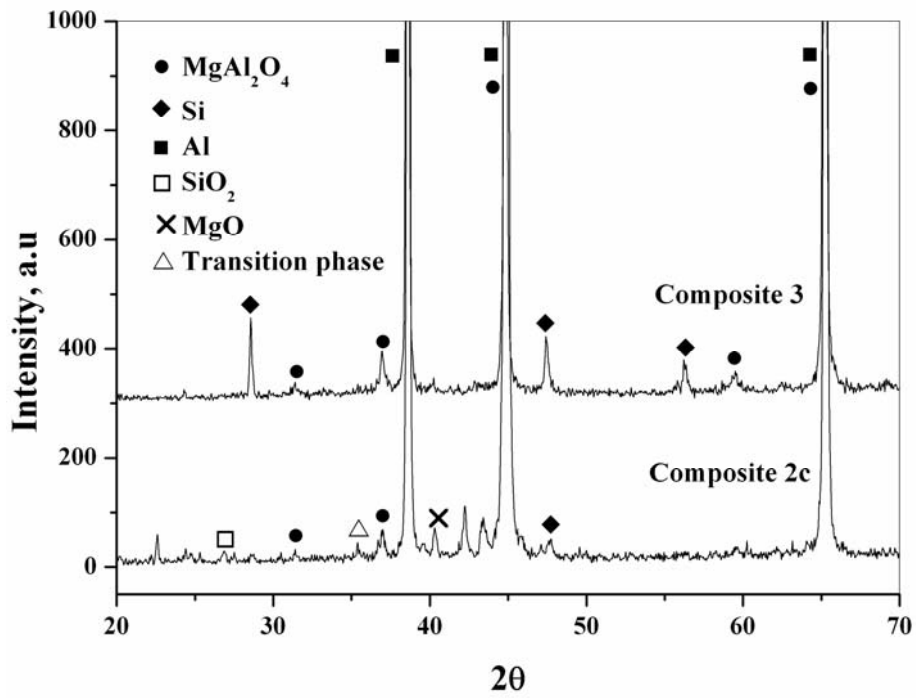


Fig.5 X-ray diffraction patterns showing the presence of Al, Si, MgAl<sub>2</sub>O<sub>4</sub>, in composites 2c and 3. Composite 2c also shows the presence of MgO, SiO<sub>2</sub> and transition phases.

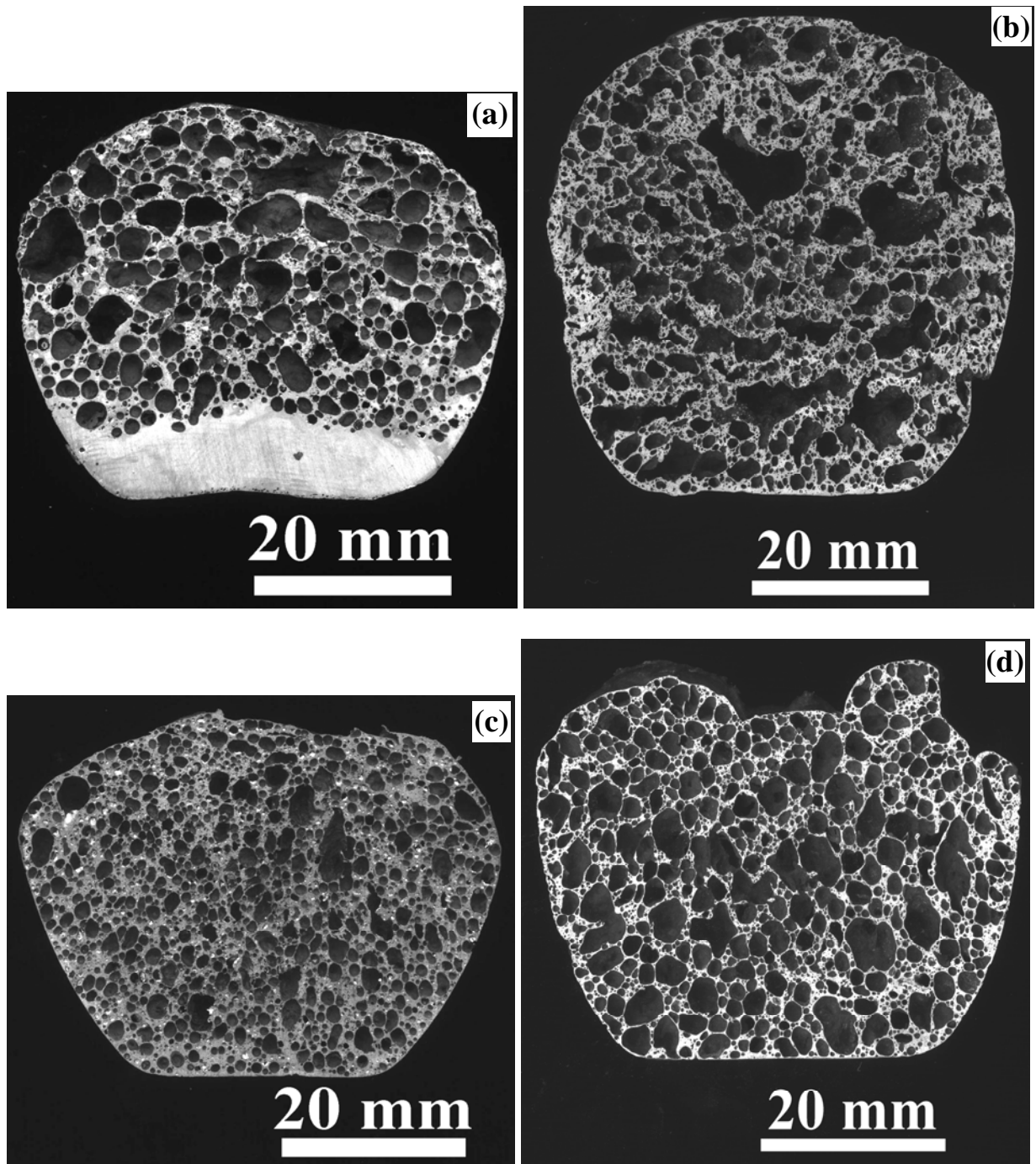


Fig.6 Cross sectional macrographs of foams produced using (a) composite 1c (b) composite 2a (c) composite 2c and (d) composite 3. The foams were made through uninterrupted foaming using untreated  $\text{TiH}_2$ , mixing time 100s, holding time 200s. The details of foaming are given in Table 2.

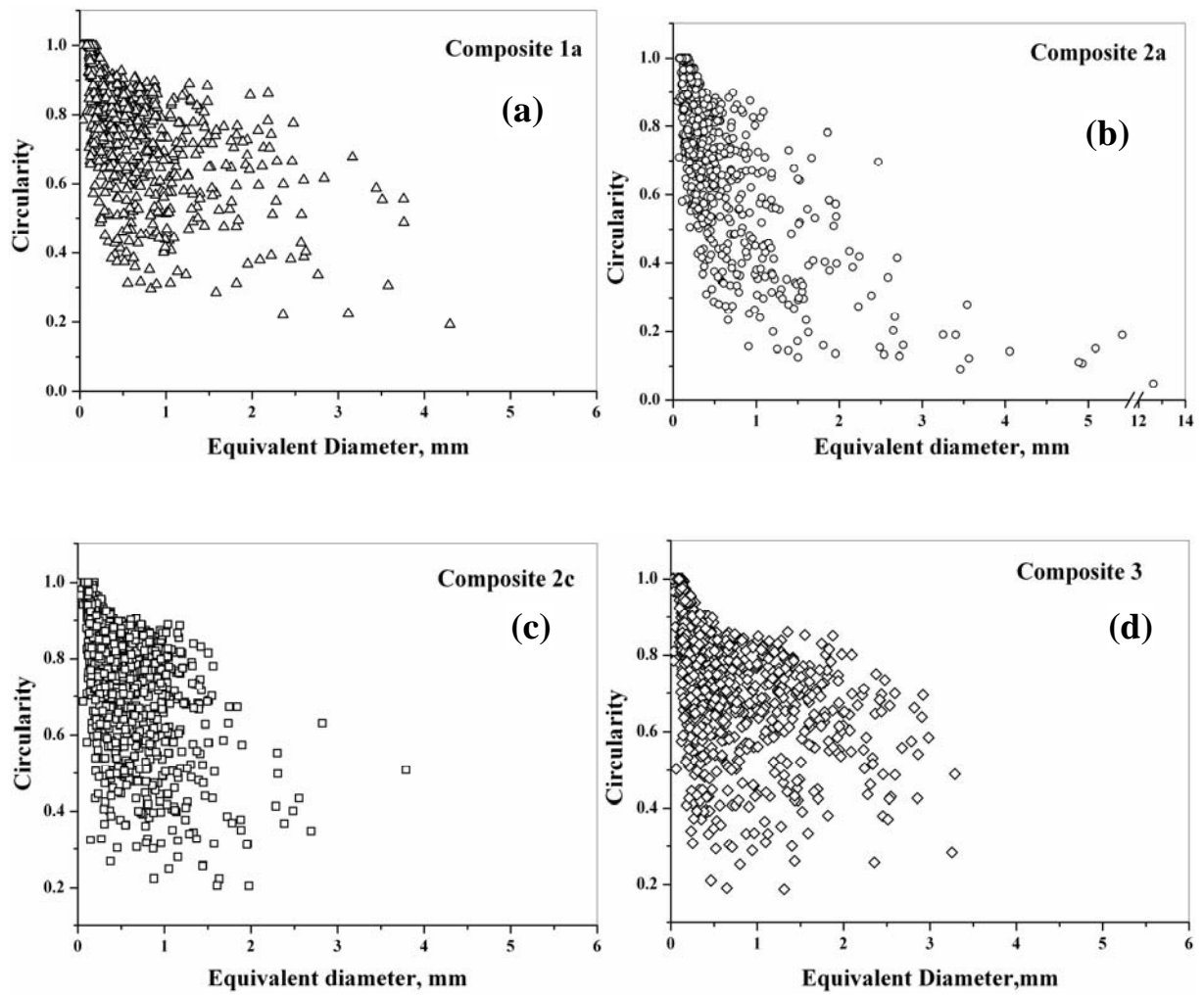


Fig.7 Circularity vs. equivalent diameter of the cells in the foams made from (a) composite 1a, (b) composite 2a (c) composite 2c and (d) composite 3.

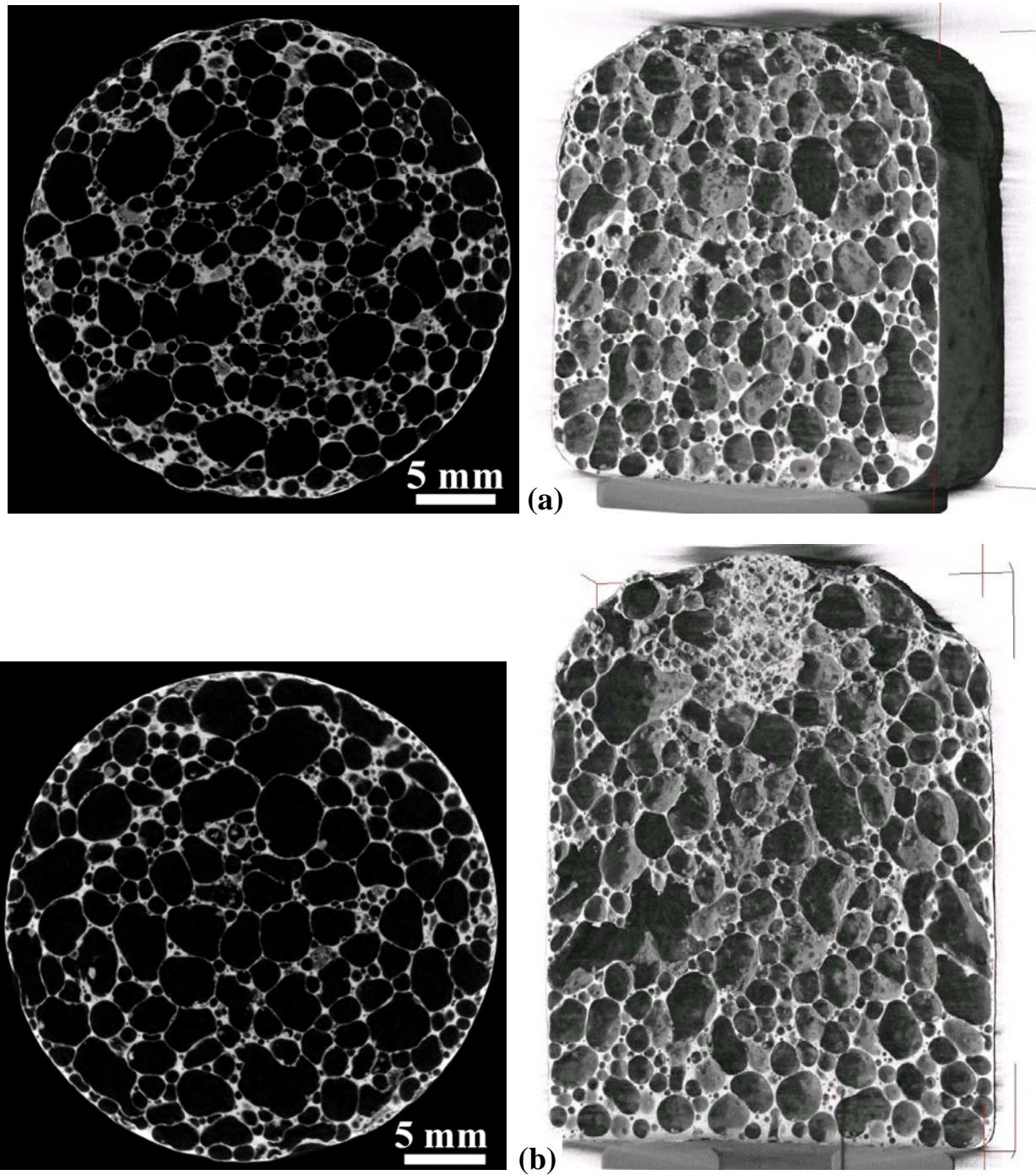


Fig.8 2D and 3D X-ray tomographic reconstruction of transverse and longitudinal sections of composite 3 foams baked in a closed steel mould at 675°C (40 mm diameter and 50 mm height). (a) baking time 300 s, porosity  $\approx 0.74$  (b) baking time 480 s, porosity  $\approx 0.80$ .

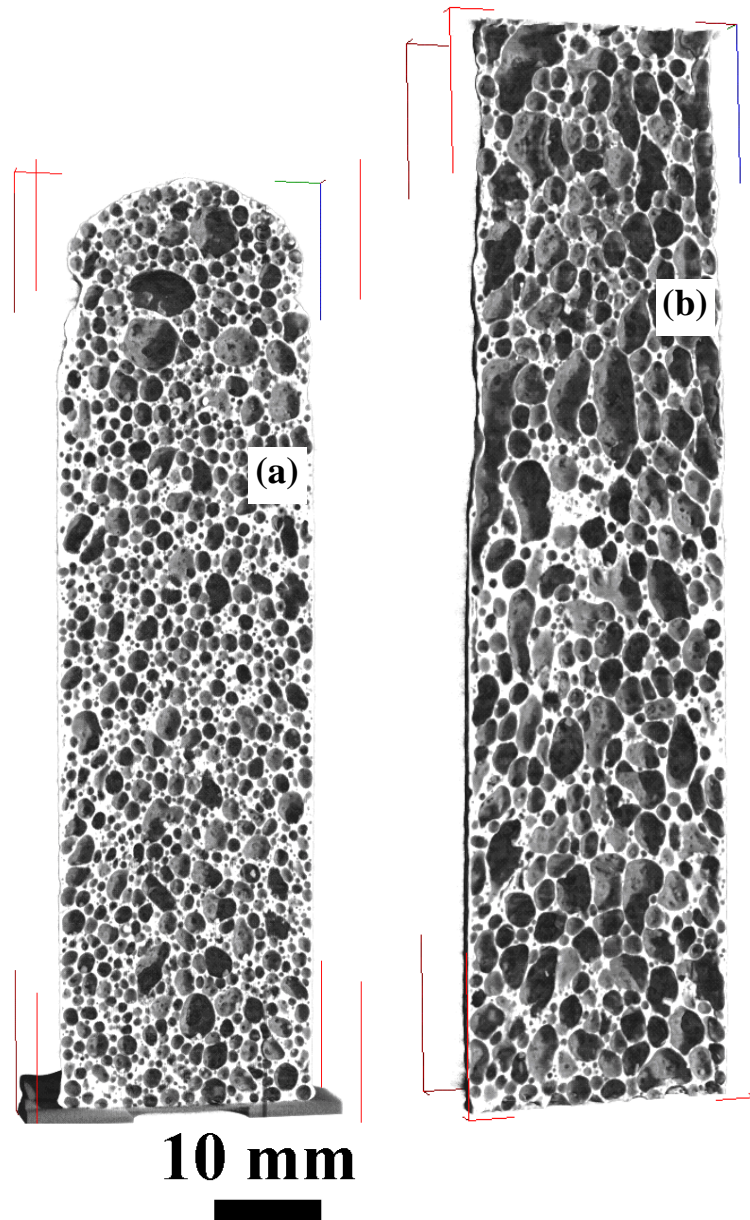


Fig.9 3D X-ray tomographic reconstruction of longitudinal cross section of composite 3 foams baked in an open steel mould at 740°C (25mm diameter and 150 mm height). (a) baking time 100 s, porosity  $\approx 0.67$  and, (b) baking time 150 s, porosity  $\approx 0.75$ . The top dome of the second foam was destroyed during blowing air for solidification. The volume expansion of the foams obtained after 100 s and 150 s with respect to the original precursor volume is 3 times and 4 times, respectively.

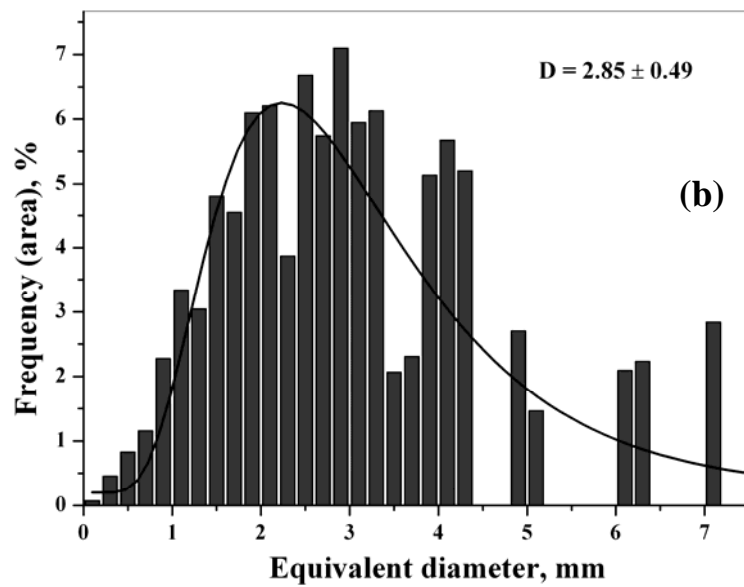
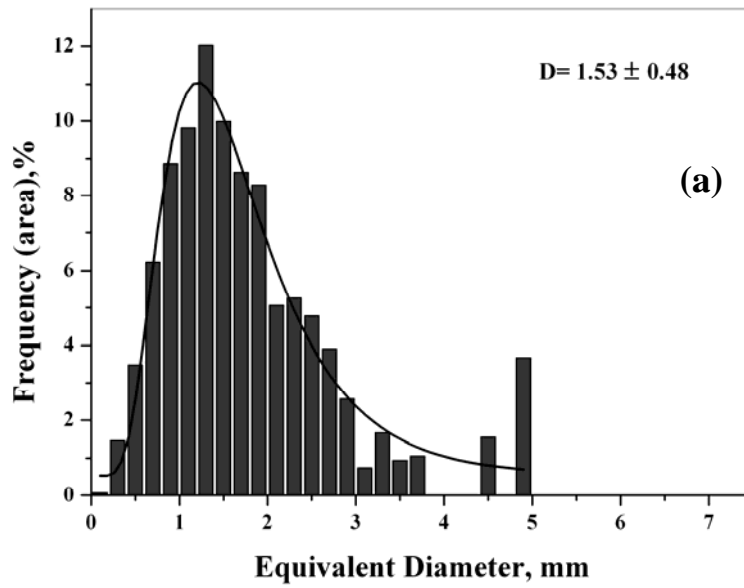


Fig.10 2D cell size distribution for composite-3 foams baked in an open steel mould (25mm diameter and 150 mm height) at 740°C for, (a) 100 s (b) 150 s.



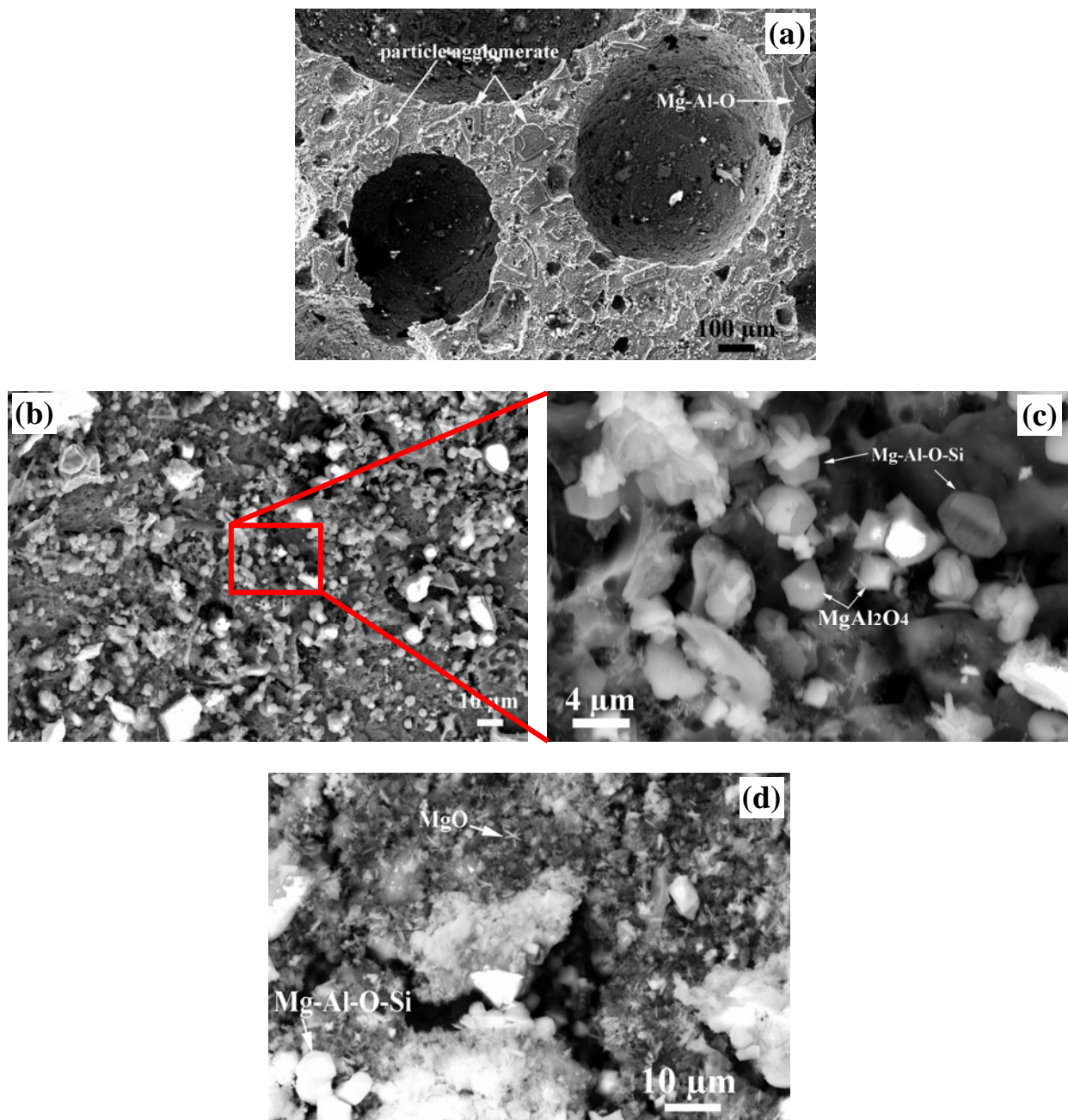


Fig.11 SEM micrographs of the cross section of cells of composite 2c foam. (a) Cross section of a cell wall, (b) inner cell surface covered with Mg-Al-O-Si and few MgAl<sub>2</sub>O<sub>4</sub> particles, (c) higher magnification revealing particles on the inner cell surface, (d) another region of cell surface showing fine needle-shaped MgO particles and spherical Mg-Al-O-Si phase.

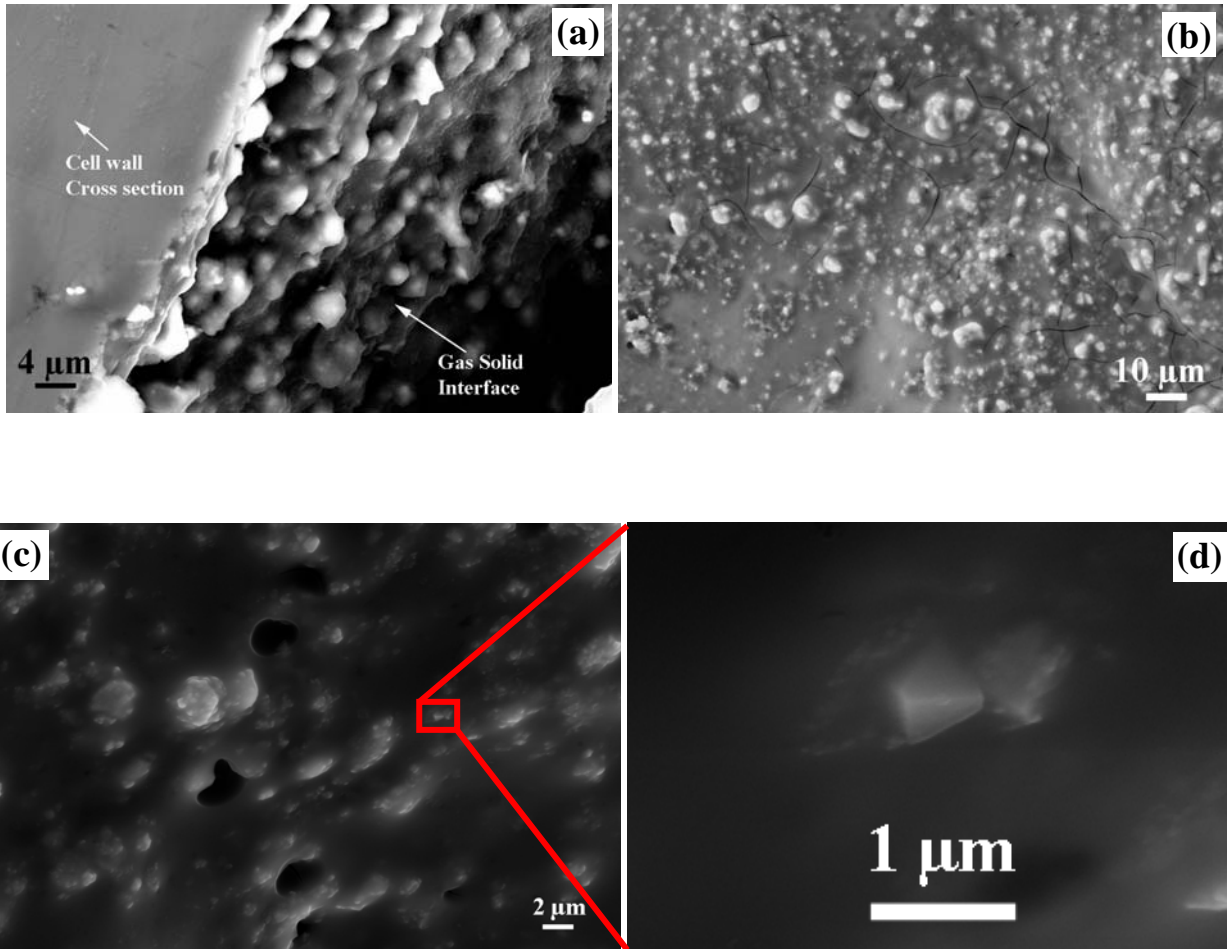


Fig.12 SEM micrographs of the inner surface of cells of composite 3 foam. (a) Cross section of a cell wall and inner cell surface covered with  $\text{MgAl}_2\text{O}_4$  particles, (b) embedded particles at the cell surface, (c) higher magnification of inner cell surface (d) a  $\text{MgAl}_2\text{O}_4$  (octahedral crystal) particle on the cell surface. Since these particles are finer it was more difficult to preserve the arrangement of particles at the edge of the cell wall while polishing the cross section.

### Cell wall cross sections

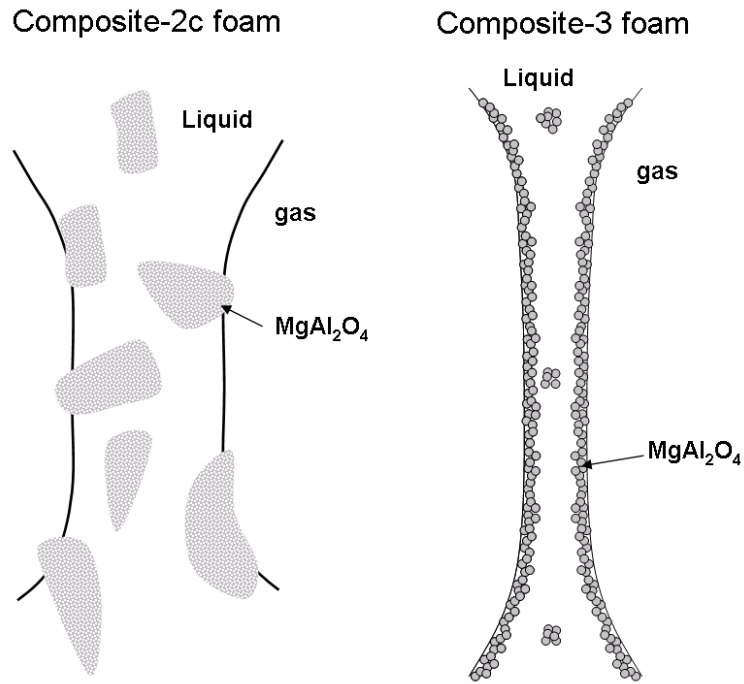


Fig.13 Idealised schematic of cell wall cross section of composite 2c and composite 3 foams showing the arrangement of the stabilizing particles inside the film and in the gas solid interface.